Diffusion and Solid Dissolution/Precipitation in Permeable Media

We have developed an analytical solution which describes mineral zonation caused by diffusion in permeable media. For a semiinfinite domain, the species conservation equations transform into ordinary differential equations that yield a closed-form solution. The solution exhibits shock dissolution/precipitation fronts and gradual (nonshock) precipitation fronts. The solution can exhibit regions (gaps) containing no reactive solids which separate moving dissolution and precipitation fronts. The analysis is, in principle, extendable to include intraaqueous reactions, although the mathematics quickly becomes intractable.

Numerical simulation exhibits all of the features of the more restricted analytical solution and is in good agreement with the data on hydroxyapatite dissolution taken by Kim and Cussler (1987).

Craig F. Novak
Robert S. Schechter
Department of Chemical Engineering

Larry W. Lake
Department of Petroleum Engineering
University of Texas
Austin, TX 78712

Introduction

Diffusion-induced mineral zonation is an important phenomenon in metasomatic processes (processes involving changes in the chemical composition of rock), causing replacement of an initial suite of minerals in a permeable medium with one or more regions of different mineral combinations. Systems such as the dissolution of hydroxyapatite (Kim and Cussler, 1987) have been experimentally examined, and some geochemical systems have been analyzed mathematically (Cussler et al., 1983; Lichtner et al., 1986 a, b; Kopinsky et al., 1988). While the convection-dominated analog to this problem has been studied extensively (Bryant, 1986; Bryant et al., 1986, 1987; Dria, 1988; Lichtner, 1985; Schechter et al., 1987; Walsh, 1983; Walsh et al., 1982, 1984), the diffusion-only regime has not received the same rigorous treatment.

The diffusion problem is generally divided into two categories:

- Interdiffusion (diffusion through both faces of a medium of finite length)
- Unidirectional diffusion (diffusion into a semiinfinite medium)

Helfferich and Katchalsky (1970) examine interdiffusion analytically, and Lichtner et al. (1986b) describe numerical and analytical solution methods for solving complex zonation problems with interdiffusion. Unidirectional diffusion has been examined both analytically and numerically. Cussler et al. (1983) develop a criterion which controls whether a solid will dissolve or precipitate in a permeable medium based upon simplified reaction stoichiometry. Lichtner et al. (1986a) consider analytical solutions to problems with one dissolution front, and also discuss numerical simulations. The above works assume local equilibrium and equal diffusion coefficients. Kopinsky et al. (1988) examine a system with one dissolution front from a finite-rate perspective and also relax the assumption of equal diffusion coefficients.

In this paper we address the problem of zonation by unidirectional diffusion. In these processes there is diffusion into a permeable medium containing an initial assemblage of minerals at a uniform concentration. The aqueous phase composition is fixed at one boundary, such as occurs when an aqueous phase flows parallel to one face of the permeable medium, maintaining a constant composition at that face. Diffusion processes are thereby initiated and certain of the resident minerals may begin to dissolve while others precipitate. The critical issues are to determine the sequence of the minerals that will appear and to locate their positions as functions of time. Regions containing no soluble solids may appear, separating zones of soluble minerals. These provide information as to the composition of the flowing aqueous phase and may help delineate the chemical history of an existing ore body.

The problem posed here is susceptible to an analytical solution under very reasonable assumptions. However, its practical application is limited to systems without significant aqueous phase speciation because these require solution of high-order and fractional-order polynomial equations. These cases require

Correspondence concerning this paper should be addressed to R. S. Schechter.

numerical solution. This solution, which compares well with analytical solutions, is applied to approximate the data of Kim and Cussler (1987).

Solution Procedure

The system

The system under study is a semiinfinite ($0 \le x \le \infty$), one-dimensional permeable medium. At the initial time the medium contains a uniform concentration of one or more reactive solids and a fluid phase in equilibrium with these minerals. At $t > 0$ the medium is perturbed by imposing, as a boundary condition, a constant-composition aqueous solution that is allowed to diffuse across the $x = 0$ boundary.

When the composition maintained at the $x = 0$ boundary is undersaturated with respect to one or more minerals in the medium, these solids will dissolve and their component species will ultimately diffuse out of the medium. This process may cause the precipitation of other solids, creating distinct zones or regions characterized by the identities of the solids present. Regions containing no reactive solids at all may also occur and are called gaps.

The point in space at which solids appear or disappear is called a diffusion front or boundary, of which there are three types: shock dissolution, shock precipitation, and gradual precipitation fronts. When, in the direction of increasing distance from the $x = 0$ boundary, a solid appears but none disappears, that front is a dissolution front. Precipitation fronts are those for which a solid disappears when moving away from the $x = 0$ boundary. These two front types can occur together, forming dissolution/precipitation fronts. Gradual precipitation fronts are characterized by a solid concentration which decreases smoothly to zero at the front.

The medium ultimately becomes partitioned into zones of constant mineral identities separated from each other by moving fronts (boundaries). The problem is to find the mineral compositions in each zone, the positions of the fronts as functions of time, and the aqueous and solid phases concentrations within each zone.

Assumptions

Since we are primarily interested in the chemistry of the system, we make a number of assumptions, many of which can be relaxed, to simplify the physics of the problem. These assumptions are common in geochemical modeling (Stohs, 1986; Walsh, 1983; Lichtner, 1985; Lichtner et al., 1986a; Cussler, 1982; Cussler et al., 1983).

1) The system is a one-dimensional, isothermal medium.

2) The fluid and solid phases are in local equilibrium. Local equilibrium in this context means that diffusion to (or from) and reaction with a solid surface occur much faster than diffusion of species through the pore space.

3) The volume fraction of soluble solids in the permeable medium is so small as to be negligible compared to the void fraction, i.e. the porosity is constant.

4) There is no convection (advection); all transport is by diffusion.

5) The same concentration-independent diffusion coefficient applies to all species.

Mathematical formulation

Consider a system with minerals S_k, $k = 1, \ldots,$ K and aqueous species σ_j, $j = 1, \ldots, J$, composed of I chemical elements. The elemental totals in the aqueous phase are given by

$$C_i \equiv \sum_{j=1}^{J} d_{ij}\sigma_j \quad i = 1, \ldots, I \tag{1}$$

where d_{ij} is a member of the aqueous stoichiometric matrix, indicating the number of atoms of the ith element in one molecule of the jth aqueous species. The elemental totals in the solid phase are similarly given by

$$\bar{C}_i \equiv \sum_{k=1}^{K} f_{ik}S_k \quad i = 1, \ldots, I \tag{2}$$

where f_{ik} is a member of the solid stoichiometric matrix, which has a definition parallel to that of the aqueous stoichiometric matrix.

The appropriate material balance is the diffusion equation

$$\frac{\partial\left(\sum_{j=1}^{J} d_{ij}\sigma_j + \sum_{k=1}^{K} f_{ik}S_k\right)}{\partial t} = \frac{\partial}{\partial x}\sum_{j=1}^{J} D\frac{\partial(d_{ij}\sigma_j)}{\partial x} \qquad i = 1, \ldots, I \tag{3}$$

where D is the effective binary molecular diffusion coefficient (Bird et al., 1960) divided by the product of medium porosity and tortuosity. The latter correction is to account for diffusion within pore spaces (Perkins and Johnston, 1963). Defining the Boltzmann transformation variable as

$$\eta \equiv \frac{1}{2\sqrt{D}}\frac{x}{\sqrt{t}}$$

the material balance, Eq. 3, becomes the ordinary differential equation

$$\frac{d\left(\sum_{j=1}^{J} d_{ij}\sigma_j + \sum_{k=1}^{K} f_{ik}S_k\right)}{d\eta} + \frac{1}{2\eta}\frac{d^2}{d\eta^2}\sum_{j=1}^{J} d_{ij}\sigma_j = 0 \quad i = 1, \ldots, I$$

Or, using the total element concentrations defined by Eqs. 1 and 2,

$$\frac{dC_i}{d\eta} + \frac{d\bar{C}_i}{d\eta} + \frac{1}{2\eta}\frac{d^2C_i}{d\eta^2} = 0 \quad i = 1, \ldots, I \tag{4}$$

Defining the operator

$$H \equiv \frac{d}{d\eta} + \frac{1}{2\eta}\frac{d^2}{d\eta^2}$$

Equation 4 becomes

$$H(C_i) + \frac{d\bar{C}_i}{d\eta} = 0 \quad i = 1, \ldots, I$$

and when all solids are absent this reduces to

$$H(C_i) = 0 \quad i = 1, \ldots, I$$

We note for future application that the equation $H(z) = 0$ has, for semi-infinite boundary conditions, the general solution

$$z = a\,\mathrm{erf}(\eta) + b$$

where a and b are constants of integration and

$$\mathrm{erf}(\eta) \equiv \frac{2}{\sqrt{\pi}} \int_0^{\eta} \exp(-\xi^2)\, d\xi$$

is the error function.

Matching conditions at moving boundaries

Matching conditions at moving (internal) fronts are required for a unique solution of moving boundary problems. These boundaries, which move in x-t space but are stationary in η space, have positions designated as η_m, $m = 1, \ldots, M$, and partition the domain into $M + 1$ zones, designated by R_r, $r = 1, \ldots, M + 1$. Two conditions are required at such boundaries: continuity of concentration and conservation of mass (a flux condition).

Aqueous concentrations must be continuous at each front, so

$$C_i^m|_{\eta_m^-} = C_i^{m+1}|_{\eta_m^+} \quad i = 1, \ldots, I \quad m = 1, \ldots, M \qquad (5)$$

where η_m is the coordinate value (position) of the mth internal boundary and $\eta_m^+ > \eta_m^-$. The superscripts indicate concentrations in the mth and $(m + 1)$th regions. Note that continuous total aqueous elemental concentrations and local equilibrium force individual species concentrations to be continuous.

The equation describing conservation of mass at discontinuous moving boundaries is commonly called the *Stefan* condition

$$\left(\frac{dC_i^m}{d\eta}\right)_{\eta_m^-} - \left(\frac{dC_i^{m+1}}{d\eta}\right)_{\eta_m^+} = -2\eta_m[(\bar{C}_i^m)_{\eta_m^-} - (\bar{C}_i^{m+1})_{\eta_m^+}]$$
$$i = 1, \ldots, I \quad m = 1, \ldots, M \qquad (6)$$

which includes both the solids dissolving at the boundary $(\bar{C}_i^{m+1})_{\eta_m^+}$, and the solids precipitating at the boundary $(\bar{C}_i^m)_{\eta_m^-}$. Note that when the solid concentrations are continuous this equation is trivial. Equation 6 can be derived in its general form (in x-t space and then transformed to η space) analogously to the heat transport problem given in Crank (1984). The Stefan condition for a dissolving solid in the diffusion problem is presented by Lichtner et al. (1986a), where it is called a Rankine-Hugoniot equation. Since this condition must be satisfied for each element, Eq. 6 resembles the coherence condition which is applied to chromatographic waves (Rhee et al., 1970) and precipitation/dissolution waves in convection problems (see for example Bryant et al., 1987).

We mention here that a condition precluding a discontinuity in solid concentration is needed when a solid precipitates at a front where no solids dissolve. A primary consequence of this condition is that the aqueous concentrations of those elements comprising the precipitating solid must have continuous first derivatives at the boundary. We examine this condition in detail below where it arises, and prove this result for a simple case in the appendix.

Formalized boundary and initial conditions

The medium is initially at constant composition, therefore

$$\bar{C}_i^{M+1} = \bar{C}_i^I \quad i = 1, \ldots, I \quad \left\{\begin{matrix} t > 0 & x \to \infty \\ t = 0 & x > 0 \end{matrix}\right\} \Longrightarrow \eta \to \infty$$

$$C_i^{M+1} = C_i^I \quad i = 1, \ldots, I \quad \left\{\begin{matrix} t > 0 & x \to \infty \\ t = 0 & x > 0 \end{matrix}\right\} \Longrightarrow \eta \to \infty$$

and the constant boundary conditions are

$$C_i^{(1)} = C_i^J \quad i = 1, \ldots, I \quad t > 0, x = 0 \Longrightarrow \eta = 0$$

Here we are using the convention that the initial condition is designated by a superscript I on concentrations and the $\eta = 0$ boundary condition with a superscript J. The boundary conditions should not be confused with concentrations for entire regions, which are marked with either a variable indicating region number, or a region number in parenthesis. Equivalent formulations of initial and boundary conditions can be written for the individual aqueous and solid species σ_j and S_k.

Calculating species concentrations

We have thus far essentially ignored individual aqueous and solid species amounts in favor of total concentrations for each element. Calculating species concentrations at each point in the medium is straightforward but complex given the total elemental abundances and the assumption of local equilibrium. Each of the J aqueous species and the K solids has a free energy of formation associated with its formation from the elements. Thus, at any point in the medium the individual aqueous and solid species amounts can be found by a constrained minimization of free energy per unit volume of solution subject to specified elemental abundances (or elemental totals for all phases). This "flash calculation" problem has been considered by a number of investigators. A comprehensive review of these is given by Smith and Missen (1982), and several robust and reliable techniques are available.

Solving the General Problem

As implied earlier, the solution method requires foreknowledge of the identities of the minerals in each of the $M + 1$ zones that may form. Novak et al. (1988) describe an efficient search procedure for finding mineral sequences for the convection-dominated analog to this problem which is readily adapted for diffusion-dominated problems. We consider this a separate issue and assume at this point that the correct mineral sequence is known. (The incorrect sequence will give a nonphysical result, such as a negative concentration, a solubility product violation, or an ordering of boundaries different from that assumed.)

The medium contains M fronts at η_m, $m = 1, \ldots, M$, separating the medium into R_r, $r = 1, \ldots, M + 1$, regions of invariant

mineral identities. We number regions and boundaries from left to right, thus R_1 is between $\eta = 0$ and η_1, R_2 from η_1 to η_2, etc. There are K_r minerals present in the rth region, where $K_r < I$ as required by equilibrium thermodynamics (Stumm and Morgan, 1981).

We arrive at analytical aqueous profiles by eliminating the derivatives of solid concentration from some of the I material balances, Eq. 4, as follows. Equation 4 can be written generally as

$$HC = \frac{-d}{d\eta}\bar{C} \tag{7}$$

where C and $\bar{C}$ are vectors of length I of total aqueous and total solid elemental concentrations, respectively. In this representation, some of the members of the $\bar{C}$ vector can be zero because the solids present do not contain all of the I elements. To explicitly show which solids are present, we introduce a zone-dependent, K-by-K diagonal matrix Δ^r, defined as

$$\Delta^r = \text{diag}\,(\delta_{1r}, \delta_{2r}, \ldots \delta_{Kr}) \tag{8}$$

where δ_{kr} is given by

$\delta_{kr} = 1$ when solid k is present in region r

$\delta_{kr} = 0$ otherwise

The Δ^r matrix indicates whether the kth solid is present in region r. The defining equation for $\bar{C}_i$, Eq. 2, becomes the matrix equation

$$\bar{C}^r \equiv F\,\Delta^r S^r \tag{9}$$

where F is the I-by-K solid stoichiometric matrix with elements f_{ik} and S^r is the vector of length K of individual solid concentrations in R_r. Combination of Eqs. 7 and 9 gives the material balance for region r

$$HC^r = \frac{-d}{d\eta}(F\Delta^r)S^r \tag{10}$$

where the superscript r indicates zone-dependent quantities.

In region r, there are $K_r \le K < I$ nonzero solid concentrations in the vector S^r, thus $\rho_r \le K$, where $\rho_r \equiv \text{rank}(F\,\Delta^r)$. Since we do not have a full rank matrix, we have a ρ_r set of base vectors which can be used to describe all other vectors in this space (Strang, 1980). We can thus generate ρ_r linearly independent rows of Eq. 10 as a base set, and use these to generate a set of $[I - \rho_r]$ rows which do not depend on the solid concentrations.

This procedure is accomplished mathematically by multiplying Eq. 10 by the I-by-I matrix P^r, which manipulates the rows of Eq. 10 using elementary matrix operations (i.e., row interchanges, multiplication of a row by a scalar, addition of rows), resulting in

$$H(P^rC^r) = \frac{-d}{d\eta}(P^rF\Delta^r)S^r = \frac{-d}{d\eta}\begin{pmatrix}0\\ Q^r\end{pmatrix}S^r \tag{11}$$

In Eq. 11, the right-side matrix consists of an $[I - \rho_r]$-by-K zero submatrix and a ρ_r-by-K Q^r submatrix of real constants.

This first $I - \rho_r$ rows of Eq. 11 provide the aqueous profile equations

$$H\left\{\sum_{p=1}^{I} p^r_{ip}C^r_p\right\} = 0 \qquad i = 1, \ldots, I - \rho_r \quad r = 1, \ldots, M + 1 \tag{12}$$

which have the solutions

$$\sum_{p=1}^{I} p^r_{ip}C^r_p = a^r_i \,\text{erf}\,(\eta) + b^r_i \qquad i = 1, \ldots, I - \rho_r \quad r = 1, \ldots, M + 1 \tag{13}$$

The remaining ρ_r rows of Eq. 11, i.e., $i = I - \rho_r + 1, I$, which depend on the solid concentrations, form a linearly independent set of equations for determining solid profiles. This is accomplished by direct integration of the last ρ_r rows of Eq. 11, i.e.

$$\int_{\eta}^{\eta_m} \frac{-d}{d\eta}\left\{\sum_{q=1}^{I} q^r_{iq}S^r_q\right\} d\eta = \int_{\eta}^{\eta_m} H\left\{\sum_{p=1}^{I} p^r_{ip}C^r_p\right\} d\eta \qquad \eta_{m-1} \le \eta < \eta_m \quad i = I - \rho_r + 1, \ldots, I \quad r = 1, \ldots, M + 1$$

or

$$\sum_{q=1}^{I} q^r_{iq}S^r_q\Big|_{\eta_m}^{\eta} = \int_{\eta}^{\eta_m} H\left\{\sum_{p=1}^{I} p^r_{ip}C^r_p\right\} d\eta \qquad \eta_{m-1} \le \eta < \eta_m \quad i = I - \rho_r + 1, \ldots, I \quad r = 1, \ldots, M + 1 \tag{14}$$

where the minus sign has been absorbed by interchanging the limits on the left side. Imbedded in these solid integral equations are another set of constants, the solid concentration at the lower limit of R_r, i.e.

$$\sum_{q=1}^{I} q^r_{iq}S^r_q\Big|_{\eta_{m-1}}^{\eta_m} = \int_{\eta_{m-1}}^{\eta_m} H\left\{\sum_{p=1}^{I} p^r_{ip}C^r_p\right\} d\eta \qquad i = I - \rho_r + 1, I \quad r = 1, \ldots, M + 1 \tag{15}$$

To summarize, each of the $M + 1$ zones contains $2\rho_r$ unknown solid constants (at the boundaries) and $2(I - \rho_r)$ unknown aqueous constants (a_i and b_i for each species). Including the M unknown boundary positions η_m gives a total of $2I(M + 1) + M$ unknowns for the M boundary, I element problem.

Finding sufficient boundary and matching conditions

Counting equations needed for solving for the unknown constants is less simple than writing equations for the profiles, Eqs. 13 and 14, because the equations depend on the sequence of minerals in a particular problem. In many cases, linear dependence among the Stefan conditions leads to an apparent overspecification. In cases with precipitation-only fronts, a condition preventing discontinuous changes in solid concentrations (i.e. requiring a gradual precipitation front) must be invoked. We present the procedure for determining the set of equations needed to find all constants by examples.

There are I Stefan conditions and I concentration matching conditions at each boundary. There are $(I - \rho_{M+1})$ independent aqueous initial conditions and ρ_{M+1} independent solid initial con-

ditions. There will be $(I - \rho_1)$ independent aqueous boundary conditions for R_1, i.e., there are no boundary condition constraints on solid concentrations for those solids with which the boundary solution is saturated. To these are added the $\Sigma_{r=1}^{M+1} \rho_r$ solid integral equations, Eq. 15, and the restriction on precipitation-only front(s), if applicable, to complete the specification. Unknowns and equations are itemized in Table 1.

Example Applications of Theory

In this section we apply the preceding theory to some simple cases.

The general problem

The steps for approaching the general problem are:

1. Assume a solid sequence.
2. Write aqueous and solid profiles for each zone, i.e., Eqs. 13 and 14.
3. Write matching conditions, Stefan conditions, boundary conditions, and initial conditions.
4. Solve the equations simultaneously.

The results of the above four steps will either indicate that the incorrect sequence was assumed in step 1, if a physical contradiction is encountered, or confirm the sequence by providing the desired solution.

The AB dissolution problem

We first examine the case of a single solid dissolved by an undersaturated aqueous solution. This is a case solved by Lichtner et al. (1986a). At $t = 0$ the medium contains species A^+, B^-, C^-, D^+ and AB(s) at concentrations C_A^I, C_B^I, C_C^I, C_D^I, and S_{AB}^I, respectively. Species A can be associated with a cation such as Ca^{2+}, species B with CO_3^{2-}, etc. We neglect speciation so that aqueous elemental totals are the same as aqueous species amounts. The only pertinent equilibria ($K = 1$) is the formation of solid AB,

$$A^+ + B^- \leftrightarrow AB(s)$$

with the solubility product relationship

$$C_A C_B = K_{AB}^{sp}$$

Since we require charge neutrality, we can eliminate the anion C^- concentration (arbitrarily) from consideration by requiring

$$C_C = C_A - C_B + C_D$$

and thus $I = 3$. For boundary conditions such that $C_A^J C_B^J < K_{AB}^{sp}$, the initial solid will dissolve. The medium will thus be divided into two regions by $M = 1$ boundaries, R_1 containing no solids, and R_2 containing solid AB, as shown in Figure 1.

Region R_1 is free of reactive solids, so the aqueous profiles are error function solutions. In region R_2, Eq. 10 is

$$H\begin{pmatrix} C_A^{(2)} \\ C_B^{(2)} \\ C_D^{(2)} \end{pmatrix} = \frac{-d}{d\eta}\left[\begin{pmatrix} 1 \\ 1 \\ 0 \end{pmatrix}(1)(S_{AB}^{(2)})\right]$$

Note that the superscript (2) indicates quantities in zone 2. The rank of $(F\Delta^{(2)})$ is 1, so there are $3 - 1 = 2$ independent equations for the aqueous profiles in R_2. One possible way to write Eq. 11 for this case is

$$H\begin{pmatrix} C_A^{(2)} - C_B^{(2)} \\ C_D^{(2)} \\ C_A^{(2)} \end{pmatrix} = \frac{-d}{d\eta}\left[\begin{pmatrix} 0 \\ 0 \\ 1 \end{pmatrix}(S_{AB}^{(2)})\right] \tag{16}$$

and Eq. 13 becomes

$$H\begin{pmatrix} C_A^{(2)} - C_B^{(2)} \\ C_D^{(2)} \end{pmatrix} = \mathbf{0}$$

Table 1. Integration Constants and Boundary and Initial Conditions for the *I*-Element, *M*-Boundary Problem

Source of Constants	Number of Constants
Aqueous Profiles	$2\sum_{r=1}^{M+1}(I - \rho_r)$
Solid Profiles	$2\sum_{r=1}^{M+1}\rho_r$
Boundary Positions	M
Total Numbers of Constants	$2I(M + 1) + M$
Type of Equations	**Number of Equations***
Initial Conditions: Aqueous	$I - \rho_{M+1}$
Initial Conditions: Solid	ρ_{M+1}
Injected Conditions: Aqueous	$I - \rho_1$
Concentration Matching at Boundaries	$M(I)$
Stefan Conditions	$M(I)$
Solid Integrals	$\sum_{r=1}^{M+1}\rho_r$
Total Number of Equations	$2I(M + 1) + \sum_{r=2}^{M+1}\rho_r$

*For problems without gradual precipitation fronts, $M = \Sigma_{r=2}^{M+1}\rho_r$. For problems with gradual precipitation fronts, there will be $M - \Sigma_{r=2}^{M+1}\rho_r$ precipitation-only wave conditions.

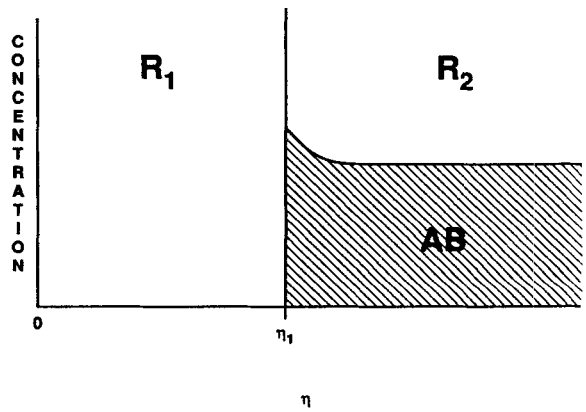

Figure 1. Solid concentration profile for the diffusion-dominated dissolution of the generalized mineral *AB* in a permeable medium.

which gives the following aqueous profiles in R_2

$$C_A^{(2)} - C_B^{(2)} = a_1^{(2)} \operatorname{erf}(\eta) + b_1^{(2)} \quad \eta \geq \eta_1$$

$$C_D^{(2)} = a_2^{(2)} \operatorname{erf}(\eta) + b_2^{(2)} \quad \eta \geq \eta_1$$

The solid profile in R_2 can be found by first solving for the A aqueous profile in R_2 using the solubility product relationship and the $C_A^{(2)} - C_B^{(2)}$ profile, i.e., by solving the quadratic equation

$$C_A^{(2)} - \frac{K_{AB}^{sp}}{C_A^{(2)}} = a_1^{(2)} \operatorname{erf}(\eta) + b_1^{(2)}$$

The resulting equation is inserted into the integrated form of the last row of Eq. 16,

$$S_{AB}^{(2)}|_\eta - S_{AB}^I = \int_\eta^\infty H \left\{ \sum_{p=1}^{I} p_{ip}^{(2)} C_p^{(2)} \right\} d\eta$$

(cf. Eq. 14). Recall that the initial condition is the limit as η approaches infinity. Aqueous and solid profiles for this problem are summarized in Table 2.

The equations which yield the constants of integration, Table 3, are generated as follows. We begin with three independent boundary conditions C_A^J, C_B^J, C_D^J, two independent aqueous initial conditions ($C_A^I - C_B^I$) and C_D^I, and one solid initial condition S_{AB}^I. We then write three concentration matching conditions and three Stefan conditions at the boundary, one each for elements A, B, and D. The matching conditions for D indicate that the D profile is unaffected by the dissolution of solid AB, which is intuitively correct because neither C nor D is connected through the chemistry of the problem. (A general principle is that aqueous species not involved in solid dissolution or precipitation at a particular front will have continuous first derivatives at these locations.)

Table 2. Equations for the Profiles of the AB Dissolution Problem

$0 \leq \eta \leq \eta_1$

$$C_A^{(1)} = a_1^{(1)} \operatorname{erf}(\eta) + b_1^{(1)}$$
$$C_B^{(1)} = a_2^{(1)} \operatorname{erf}(\eta) + b_2^{(1)}$$
$$C_D^{(1)} = a_3^{(1)} \operatorname{erf}(\eta) + b_3^{(1)}$$

$\eta \geq \eta_1$

$$C_A^{(2)} = \frac{[a_1^{(2)} \operatorname{erf}(\eta) + b_1^{(2)}] + \sqrt{[a_1^{(2)} \operatorname{erf}(\eta) + b_1^{(2)}]^2 + 4K_{AB}^{sp}}}{2}$$

$$C_B^{(2)} = \frac{-[a_1^{(2)} \operatorname{erf}(\eta) + b_1^{(2)}] + \sqrt{[a_1^{(2)} \operatorname{erf}(\eta) + b_1^{(2)}]^2 + 4K_{AB}^{sp}}}{2}$$

$$C_D^{(2)} = a_2^{(2)} \operatorname{erf}(\eta) + b_2^{(2)}$$

$$S_{AB}^{(2)}(\eta) - S_{AB}^I = \frac{4(a_1^{(2)})^2 K_{AB}^{sp}}{\pi} \int_\eta^\infty \frac{\exp(-2\eta^2)}{\eta \{[a_1^{(2)} \operatorname{erf}(\eta) + b_1^{(2)}]^2 + 4K_{AB}^{sp}\}^{3/2}} d\eta$$

Table 3. Boundary and Matching Conditions for the AB Dissolution Problem

Boundary and Initial Conditions

$$C_A^{(1)} = C_A^J \qquad \eta = 0$$
$$C_B^{(1)} = C_B^J \qquad \eta = 0$$
$$C_D^{(1)} = C_D^J \qquad \eta = 0$$
$$C_A^{(2)} - C_B^{(2)} = C_A^I - C_B^I \qquad \eta \to \infty$$
$$C_D^{(2)} = C_D^I \qquad \eta \to \infty$$

Concentration Matching at η_1

$$a_1^{(1)} \operatorname{erf}(\eta_1) + b_1^{(1)} = \frac{[a_1^{(2)} \operatorname{erf}(\eta_1) + b_1^{(2)}] + \sqrt{[a_1^{(2)} \operatorname{erf}(\eta_1) + b_1^{(2)}]^2 + 4K_{AB}^{sp}}}{2}$$

$$a_2^{(1)} \operatorname{erf}(\eta_1) + b_2^{(1)} = \frac{-[a_1^{(2)} \operatorname{erf}(\eta_1) + b_1^{(2)}] + \sqrt{[a_1^{(2)} \operatorname{erf}(\eta_1) + b_1^{(2)}]^2 + 4K_{AB}^{sp}}}{2}$$

$$a_3^{(1)} \operatorname{erf}(\eta_1) + b_3^{(1)} = a_2^{(2)} \operatorname{erf}(\eta_1) + b_2^{(2)}$$

Stefan Conditions at η_1

$$2a_1^{(1)} - a_1^{(2)} \left\{ \frac{a_1^{(2)} \operatorname{erf}(\eta_1) + b_1^{(2)}}{\sqrt{[a_1^{(2)} \operatorname{erf}(\eta_1) + b_1^{(2)}]^2 + 4K_{AB}^{sp}}} + 1 \right\} = (2\sqrt{\pi})\, \eta_1 \exp(\eta_1^2) S_{AB}^{(2)}|_{\eta_1}$$

$$2a_2^{(1)} - a_1^{(2)} \left\{ \frac{a_1^{(2)} \operatorname{erf}(\eta_1) + b_1^{(2)}}{\sqrt{[a_1^{(2)} \operatorname{erf}(\eta_1) + b_1^{(2)}]^2 + 4K_{AB}^{sp}}} - 1 \right\} = (2\sqrt{\pi})\, \eta_1 \exp(\eta_1^2) S_{AB}^{(2)}|_{\eta_1}$$

$$a_3^{(1)} - a_2^{(2)} = 0$$

Solid Integral Equation with lower limit η_1

$$S_{AB}^{(2)}|_{\eta_1} - S_{AB}^I = \frac{4(a_1^{(2)})^2 K_{AB}^{sp}}{\pi} \int_{\eta_1}^\infty \frac{\exp(-2\eta^2)}{\eta \{[a_1^{(2)} \operatorname{erf}(\eta) + b_1^{(2)}]^2 + 4K_{AB}^{sp}\}^{3/2}} d\eta$$

The equations in Table 3 apply for an arbitrary set of initial and boundary conditions. The solution to these equations for two values of S_{AB}^I are given in Table 4 and Figure 2, as calculated using the Newton-Raphson rootfinding algorithm. We defer a physical explanation of all results to the Discussion section of this paper.

Comparison with convection-dominated AB dissolution

The simple dissolution of AB by a diffusing solution can be easily compared to the analogous convection-dominated (no diffusion or dispersion) dissolution. Figure 3 shows composition routes for the convection-dominated case (I-I''-J) and for the diffusion-dominated case (I-I'-J'-J). The figure plots the total (solid plus aqueous) concentration of A vs. the total B concentration.

Helfferich (1989) discusses the construction of concentration routes for convection-dominated problems; we give only a brief

Table 4. Constants of Integration for the AB Dissolution Problem

Initial Conditions: $C_A^I = 2.0$; $C_B^I = 1.0$; $C_D^I = 0.4$

Injected Conditions: $C_A^J = 1.5$; $C_B^J = 0.3$; $C_D^J = 1.2$

Solubility Product: $K_{AB}^{sp} = 2.0$

	$S_{AB}^I = 0.05$	$S_{AB}^I = 0.50$
$a_1^{(1)}$	0.5414	0.8216
$a_2^{(1)}$	0.7414	1.0216
$a_3^{(1)} = a_2^{(2)}$	−0.8	−0.8
$a_1^{(2)}$	−0.2	−0.2
$b_1^{(1)}$	1.5	1.5
$b_2^{(1)}$	0.3	0.3
$b_3^{(1)} = b_2^{(2)}$	1.2	1.2
$b_1^{(2)}$	1.2	1.2
η_1	1.3230	0.6797
$S_{AB}^{(2)}\|_{\eta_1}$	0.05001	0.5005

sketch here. The convection-dominated AB dissolution problem consists of two waves, the fastest of which is a salinity wave, shown as segment I-I' in Figure 3. This is an indifferent wave (Lake, 1989) and is represented by a line of constant AB concentration passing through the initial condition I. Lines of constant solid concentration are the hyperbolic-shaped lines in Figure 3 labeled with the specific solid concentration. The last wave in the problem is a shock dissolution wave, which follows a line of unit slope (as determined by coherence) through the injected condition J. Line segment I''-J represents this wave. The paths, constant AB and coherent dissolution, are valid for any initial (I) and undersaturated injected (J) conditions.

Figure 3 shows the route for the diffusion-dominated AB dissolution problem having the same initial and injected conditions. The route consists of a curved spreading wave portion (I-I'), followed by a shock dissolution wave (I'-J'), and then a second spreading wave (J'-J). The shock portion occurs at constant aqueous concentration, as required in diffusion problems. The segments I'-J' and J'-J are set by the physics of the problem: I'-J' is along a line which satisfies the Stefan condition and J'-J is a straight line from the intersection of the previous wave segment with the saturated solid ($S_{AB} = 0$) curve. The segment I-I' is *not* a proper concentration route, however, inasmuch as a different initial condition will yield a different curve—even an initial condition along the I-I' curve. Thus the entire route I-I'-J'-J is not a true composition route in the sense described by Helfferich and Klein (1970). However, the two cases shown in Figure 3 represent extremes of convection- and diffusion-dominated behavior. All other cases fall in between these extremes.

Figure 4 shows another comparison between the convection- and diffusion-dominated cases. These figures are plots of solid and aqueous concentrations versus the variable η, which for the diffusion-dominated problem is $x/(2\sqrt{Dt})$ and for the convection-dominated problem, defined only for this comparison, is x/t. The differences in the transform variable make spatial comparisons difficult; however, there are general qualitative differences in the solutions. The convection-dominated case has discontinuities in all concentrations, but discontinuities exist only in the solid concentration for the diffusion-dominated case. The discontinuity in the latter case is caused by the absence of diffusion in the solid phase.

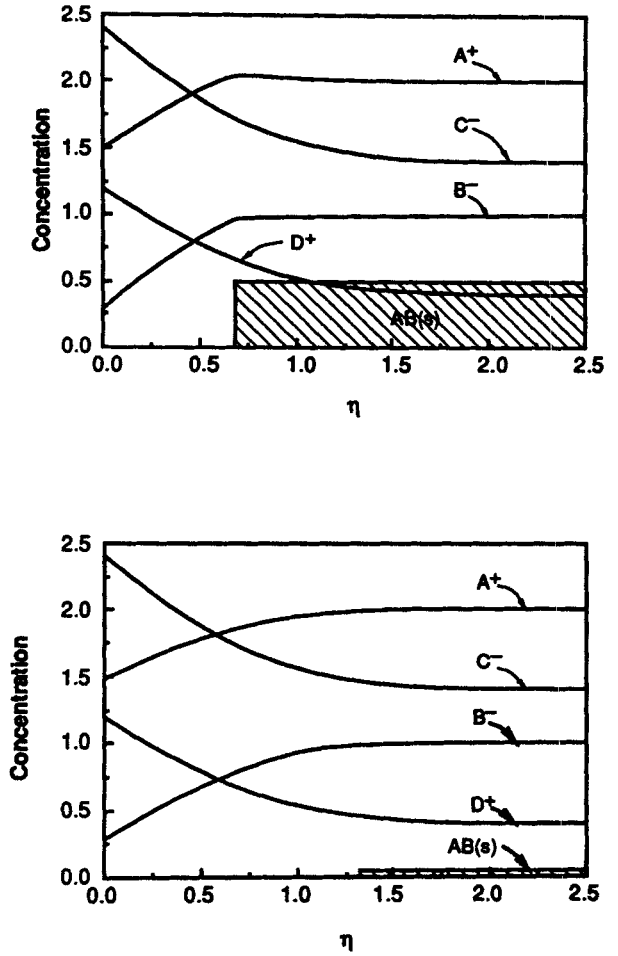

Figure 2. Solid and aqueous concentration profiles for the diffusion-dominated dissolution of solid AB for initial concentrations: (a) $S_{AB} = 0.5$ and (b) $S_{AB} = 0.05$.

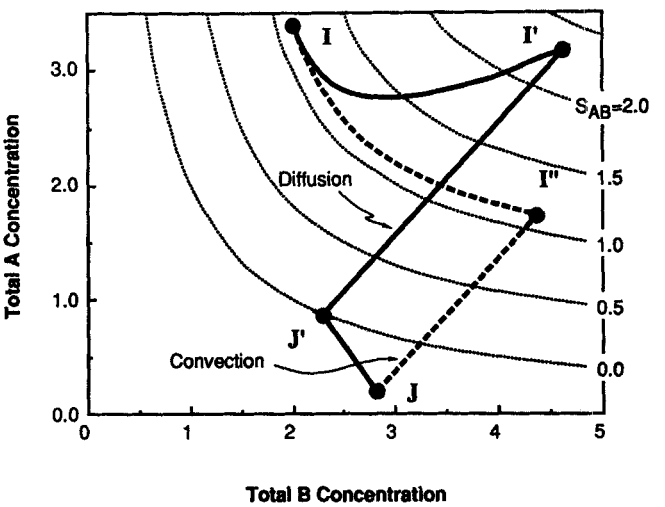

Figure 3. Composition path diagram showing composition routes for convection-dominated dissolution of AB(I-I''-J) and diffusion-dominated dissolution of AB(I-I'-J'-J).

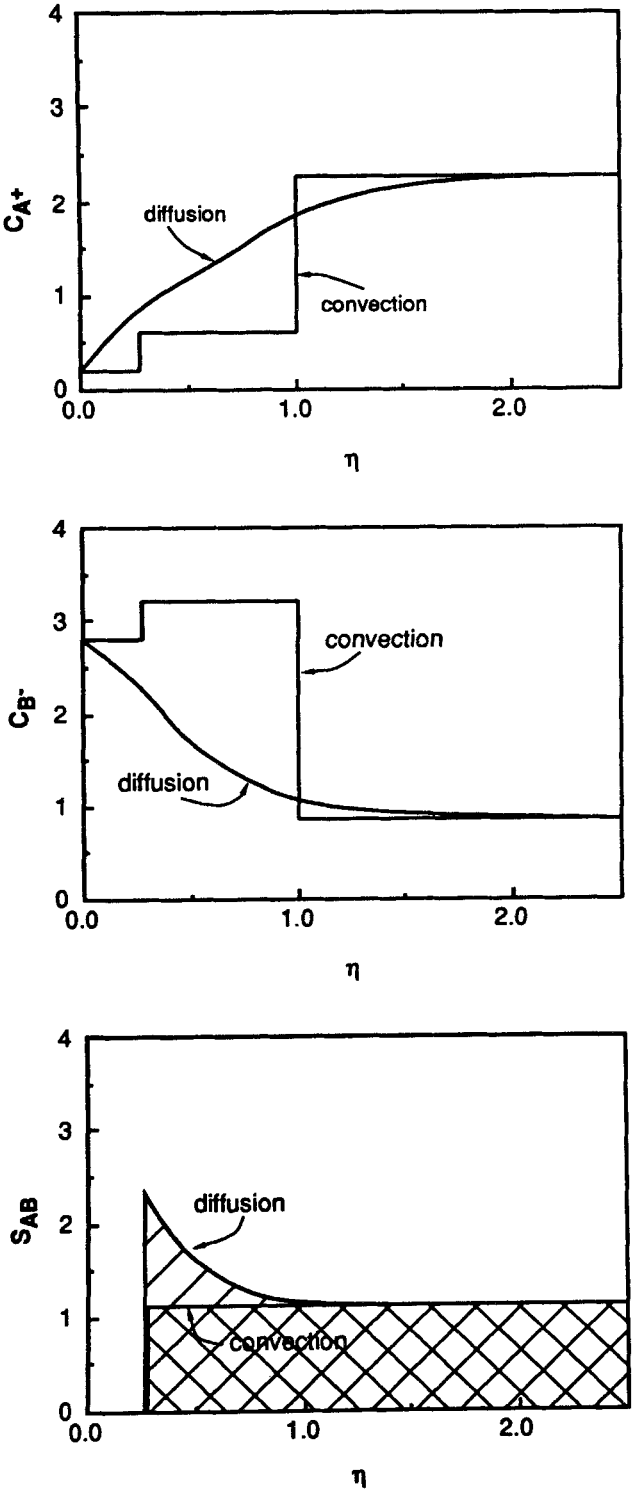

Figure 4. Solid and aqueous concentration profiles comparing convection- and diffusion-dominated dissolution of *AB*. For convection, $\eta = (x/t)$; for diffusion, $\eta = x/(2\sqrt{Dt})$.

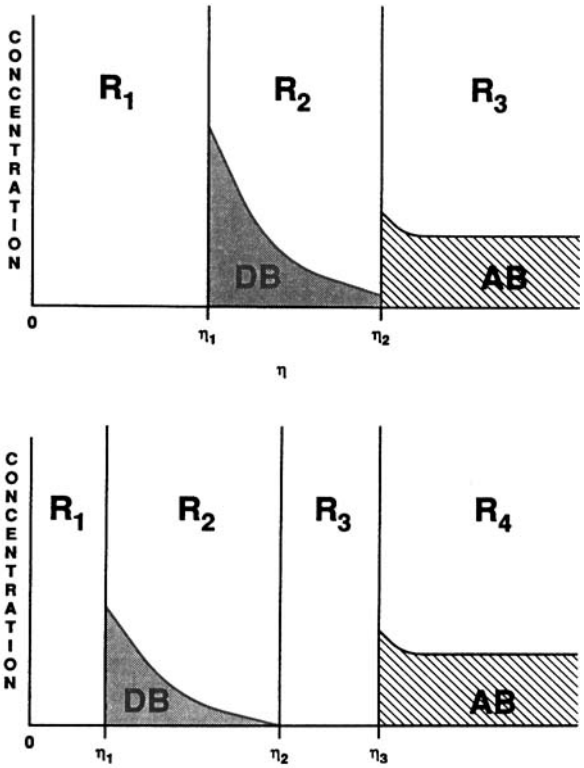

Figure 5. Solid concentration profiles for the diffusion-dominated dissolution of mineral *AB* followed by: (a) solid *DB* precipitation (R_2) and (b) a gap (R_3) and solid *DB* precipitation (R_2).

Table 5. Equations for the Aqueous Profiles of the *AB* Dissolution Problem with a Shock DB Precipitation Wave

$0 \le \eta \le \eta_1$

$$C_A^{(1)} = a_1^{(1)} \operatorname{erf}(\eta) + b_1^{(1)}$$
$$C_B^{(1)} = a_2^{(1)} \operatorname{erf}(\eta) + b_2^{(1)}$$
$$C_D^{(1)} = a_3^{(1)} \operatorname{erf}(\eta) + b_3^{(1)}$$

$\eta_1 \le \eta \le \eta_2$

$$C_A^{(2)} = a_1^{(1)} \operatorname{erf}(\eta) + b_1^{(1)} \quad \text{(Note that } a_2^{(2)} = a_1^{(1)} \text{ and } b_2^{(2)} = b_1^{(1)})$$

$$C_B^{(2)} = \frac{-[a_1^{(2)} \operatorname{erf}(\eta) + b_1^{(2)}] + \sqrt{[a_1^{(2)} \operatorname{erf}(\eta) + b_1^{(2)}]^2 + 4K_{DB}^{sp}}}{2}$$

$$C_D^{(2)} = \frac{[a_1^{(2)} \operatorname{erf}(\eta) + b_1^{(2)}] + \sqrt{[a_1^{(2)} \operatorname{erf}(\eta) + b_1^{(2)}]^2 + 4K_{DB}^{sp}}}{2}$$

$\eta \ge \eta_2$

$$C_A^{(3)} = \frac{[a_1^{(3)} \operatorname{erf}(\eta) + b_1^{(3)}] + \sqrt{[a_1^{(3)} \operatorname{erf}(\eta) + b_1^{(3)}]^2 + 4K_{AB}^{sp}}}{2}$$

$$C_B^{(3)} = \frac{-[a_1^{(3)} \operatorname{erf}(\eta) + b_1^{(3)}] + \sqrt{[a_1^{(3)} \operatorname{erf}(\eta) + b_1^{(3)}]^2 + 4K_{AB}^{sp}}}{2}$$

$$C_D^{(3)} = a_2^{(3)} \operatorname{erf}(\eta) + b_2^{(3)}$$

Two dissolution/precipitation problems

More complex system behavior can result if we allow solid DB to form,

$$D^+ + B^- \leftrightarrow DB(s)$$

$$C_D\, C_B = K_{DB}^{sp}$$

in addition to AB, so $K = 2$.

There are two possible mineral sequences in which solid DB precipitates in a medium initially containing AB. In the first case, Figure 5a, solid DB precipitates in a shock at the AB dissolution front. The other structure, Figure 5b, contains a gap between the AB dissolution front and a gradual DB precipitation front. Either structure can form depending on the initial AB concentration and the solubility product of DB. In addition, solid DB may not precipitate for all initial and boundary conditions, reverting to the metasomatic structure in Figure 2.

The Shock Precipitation Sequence

The first sequence, Figure 5a, has $M = 2$ boundaries and 3 regions. Equation 10 is

$$H\begin{pmatrix} C_A^r \\ C_B^r \\ C_D^r \end{pmatrix} = \frac{-d}{d\eta}\begin{pmatrix} 1 & 0 \\ 1 & 1 \\ 0 & 1 \end{pmatrix}\begin{pmatrix} \delta_{1r} & 0 \\ 0 & \delta_{2r} \end{pmatrix}\begin{pmatrix} S_{AB}^r \\ S_{DB}^r \end{pmatrix} \quad r = 1, 2, 3$$

In R_3, only AB is present, so $K_3 = 1$, $\Delta^{(3)} = \text{diag}\ (1, 0)$ and rank $(F\Delta^{(3)}) = 1$, which gives $3 - 1 = 2$ independent aqueous profiles for $(C_A^{(3)} - C_B^{(3)})$ and $C_D^{(3)}$. Similarly for R_2, $K_2 = 1$ $\Delta^{(2)} = \text{diag}\ (0, 1)$ and rank $(F\Delta^{(2)}) = 1$, resulting in $(C_D^{(2)} - C_B^{(2)})$ and $C_A^{(2)}$ aqueous profiles. Finally, in region $R_1\Delta^{(1)} = \text{diag}\ (0, 0)$. Table 5 contains the aqueous profile equations for this problem.

Before solving for the unknowns, we can simplify the system by recognizing that the integration constants for the C_A profile in regions R_1 and R_2 are identical because A does not participate in solid formation in either zone, as was the case for the matching conditions on species D in the previous example. There are

Table 6. Boundary and Matching Equations for the AB Dissolution Problem with a Shock DB Precipitation Front

Boundary and Initial Conditions: $b_1^{(1)} = C_A^J;\ b_2^{(1)} = C_B^J;\ b_3^{(1)} = C_D^J$

Initial Conditions: $a_1^{(3)} + b_1^{(3)} = C_A^I - C_B^I;\ a_2^{(3)} + b_2^{(3)} = C_D^I$

Concentration Matching Conditions (B and D at η_1, A, B, and D at η_2)

$$2(a_2^{(1)}\,\text{erf}\,(\eta_1) + b_2^{(1)}) = -[a_1^{(2)}\,\text{erf}\,(\eta_1) + b_1^{(2)}] + \sqrt{[a_1^{(2)}\,\text{erf}\,(\eta_1) + b_1^{(2)}]^2 + 4K_{DB}^{sp}}$$

$$2(a_3^{(1)}\,\text{erf}\,(\eta_1) + b_3^{(1)}) = [a_1^{(2)}\,\text{erf}\,(\eta_1) + b_1^{(2)}] + \sqrt{[a_1^{(2)}\,\text{erf}\,(\eta_1) + b_1^{(2)}]^2 + 4K_{DB}^{sp}}$$

$$2(a_1^{(1)}\,\text{erf}\,(\eta_2) + b_1^{(1)}) = [a_1^{(3)}\,\text{erf}\,(\eta_2) + b_1^{(3)}] + \sqrt{[a_1^{(3)}\,\text{erf}\,(\eta_2) + b_1^{(3)}]^2 + 4K_{AB}^{sp}}$$

$$-[a_1^{(2)}\,\text{erf}\,(\eta_2) + b_1^{(2)}] + \sqrt{[a_1^{(2)}\,\text{erf}\,(\eta_2) + b_1^{(2)}]^2 + 4K_{DB}^{sp}} = -[a_1^{(3)}\,\text{erf}\,(\eta_2) + b_1^{(3)}] + \sqrt{[a_1^{(3)}\,\text{erf}\,(\eta_2) + b_1^{(3)}]^2 + 4K_{AB}^{sp}}$$

$$[a_1^{(2)}\,\text{erf}\,(\eta_2) + b_1^{(2)}] + \sqrt{[a_1^{(2)}\,\text{erf}\,(\eta_2) + b_1^{(2)}]^2 + 4K_{DB}^{sp}} = 2(a_2^{(3)}\,\text{erf}\,(\eta_2) + b_2^{(3)})$$

Stefan Conditions (B and D at η_1, A, B, and D at η_2

$$2a_2^{(1)} - a_1^{(2)}\left\{\frac{a_1^{(2)}\,\text{erf}\,(\eta_1) + b_1^{(2)}}{\sqrt{[a_1^{(2)}\,\text{erf}\,(\eta_1) + b_1^{(2)}]^2 + 4K_{DB}^{sp}}} - 1\right\} = (2\sqrt{\pi})\,\eta_1 \exp(\eta_1^2) S_{DB}^{(2)}|_{\eta_1}$$

$$2a_3^{(1)} - a_1^{(2)}\left\{\frac{a_1^{(2)}\,\text{erf}\,(\eta_1) + b_1^{(2)}}{\sqrt{[a_1^{(2)}\,\text{erf}\,(\eta_1) + b_1^{(2)}]^2 + 4K_{DB}^{sp}}} + 1\right\} = (2\sqrt{\pi})\,\eta_1 \exp(\eta_1^2) S_{DB}^{(2)}|_{\eta_1}$$

$$2a_1^{(1)} - a_1^{(3)}\left\{\frac{a_1^{(3)}\,\text{erf}\,(\eta_2) + b_1^{(3)}}{\sqrt{[a_1^{(3)}\,\text{erf}\,(\eta_2) + b_1^{(3)}]^2 + 4K_{AB}^{sp}}} + 1\right\} = (2\sqrt{\pi})\,\eta_2 \exp(\eta_2^2) S_{AB}^{(3)}|_{\eta_2}$$

$$a_1^{(2)}\left\{\frac{a_1^{(2)}\,\text{erf}\,(\eta_2) + b_1^{(2)}}{\sqrt{[a_1^{(2)}\,\text{erf}\,(\eta_2) + b_1^{(2)}]^2 + 4K_{DB}^{sp}}} - 1\right\} - a_1^{(3)}\left\{\frac{a_1^{(3)}\,\text{erf}\,(\eta_2) + b_1^{(3)}}{\sqrt{[a_1^{(3)}\,\text{erf}\,(\eta_2) + b_1^{(3)}]^2 + 4K_{AB}^{sp}}} - 1\right\} = (2\sqrt{\pi})\,\eta_2 \exp(\eta_2^2)(S_{AB}^{(3)}|_{\eta_2} - S_{DB}^{(2)}|_{\eta_2})$$

$$-2a_2^{(3)} + a_1^{(2)}\left\{\frac{a_1^{(2)}\,\text{erf}\,(\eta_2) + b_1^{(2)}}{\sqrt{[a_1^{(2)}\,\text{erf}\,(\eta_2) + b_1^{(2)}]^2 + 4K_{DB}^{sp}}} + 1\right\} = -(2\sqrt{\pi})\,\eta_2 \exp(\eta_2^2) S_{DB}^{(2)}|_{\eta_2}$$

Solid Integral Equation with Limits η_1 and η_2, and η_2 and Infinity

$$S_{DB}^{(2)}|_{\eta_1} - S_{DB}^{(2)}|_{\eta_2} = \frac{4(a_1^{(2)})^2 K_{DB}^{sp}}{\pi}\int_{\eta_1}^{\eta_2} \frac{\exp(-2\eta^2)}{\eta\{[a_1^{(2)}\,\text{erf}\,(\eta) + b_1^{(2)}]^2 + 4K_{DB}^{sp}\}^{3/2}}\,d\eta$$

$$S_{AB}^{(3)}|_{\eta_2} - S_{AB}^{I} = \frac{4(a_1^{(3)})^2 K_{AB}^{sp}}{\pi}\int_{\eta_2}^{\infty} \frac{\exp(-2\eta^2)}{\eta\{[a_1^{(3)}\,\text{erf}\,(\eta) + b_1^{(3)}]^2 + 4K_{AB}^{sp}\}^{3/2}}\,d\eta$$

now three boundary conditions, two aqueous initial conditions, one solid initial condition, five concentration matching conditions, five Stefan conditions, and two solid integral equations. These are summarized in Table 6. The constants of integration for this problem, with the same initial and injected conditions as Figure 2a are shown in Table 7, and the profiles are plotted in Figure 6a.

The Gradual Precipitation Sequence

The sequence of Figure 5b is solved in much the same way, except, using the equations in Table 1, we see that the

$$2I(M + 1) + M = 2(3)(4) + 3 = 27$$

unknowns cannot be determined using the

$$[I - \text{rank}\,(F\Delta^{(1)})] + [I - \text{rank}\,(F\Delta^{(4)})] + \text{rank}\,(F\Delta^{(4)}) + M(I + I) + \sum_{r=1}^{M+1} \text{rank}\,(F\Delta^{r}) = 3 + 2 + 1 + 3(3 + 3) + 2 = 26$$

equations of the type already discussed. An additional condition is needed to overcome this apparent underspecification. For systems containing gaps between solids, the solid concentration must vanish at the end of the interval, which for this example means that $S^{(2)}_{DB}|_{\eta_2^-} = 0$. This condition forces the DB precipitation front to be a gradual precipitation front (i.e., it cannot be a shock) and forces the derivatives of aqueous species B and D concentrations to be continuous at the precipitation boundary η_2. Intuitively, there seems to be no reason why a solid should precipitate abruptly at a front where solid dissolution does not simultaneously occur. If we forced solid DB to have a nonzero concentration at η_2, aqueous concentrations to the right of the front would violate the solubility product, indicating a nonphysical result. We prove that the solid concentration must vanish at η_2 in the appendix.

Table 7. Constants of Integration for the AB Dissolution Problem with a Shock DB Precipitation Front

Initial Conditions: $C^I_A = 2.0$; $C^I_B = 1.0$; $C^I_D = 0.4$

Injected Conditions: $C^J_A = 1.5$; $C^J_B = 0.3$; $C^J_D = 1.2$

Solubility Product: $K^{sp}_{AB} = 2.0$; $K^{sp}_{DB} = 0.5$

For $S^I_{AB} = 0.50$

$a^{(1)}_1 = 0.8396$	$b^{(1)}_1 = 1.5$
$a^{(1)}_2 = 0.9043$	$b^{(1)}_2 = 0.3$
$a^{(1)}_3 = -0.9352$	$b^{(1)}_3 = 1.2$
$a^{(2)}_1 = -1.8396$	$b^{(2)}_1 = 0.9$
$a^{(3)}_1 = -0.5498$	$b^{(3)}_1 = 1.5498$
$a^{(3)}_2 = -0.4502$	$b^{(3)}_2 = 0.8502$

$\eta_1 = 0.2060$
$\eta_2 = 0.7637$
$S^{(2)}_{DB}|_{\eta_1} = 0.7329$
$S^{(2)}_{DB}|_{\eta_2} = 0.08464$
$S^{(3)}_{AB}|_{\eta_2} = 0.5023$

Table 8. Aqueous Profiles for the AB Dissolution Problem with a Gradual DB Precipitation Front

$0 \le \eta \le \eta_1$

$$C^{(1)}_A = a^{(1)}_1 \,\text{erf}\,(\eta) + b^{(1)}_1$$
$$C^{(1)}_B = a^{(1)}_2 \,\text{erf}\,(\eta) + b^{(1)}_2$$
$$C^{(1)}_D = a^{(1)}_3 \,\text{erf}\,(\eta) + b^{(1)}_3$$

$\eta_1 \le \eta \le \eta_2$

$$C^{(2)}_A = a^{(1)}_1 \,\text{erf}\,(\eta) + b^{(1)}_1$$
$$C^{(2)}_D - C^{(2)}_B = a^{(2)}_2 \,\text{erf}\,(\eta) + b^{(2)}_2$$

$\eta_2 \le \eta \le \eta_3$

$$C^{(3)}_A = a^{(1)}_1 \,\text{erf}\,(\eta) + b^{(1)}_1$$
$$C^{(3)}_B = a^{(3)}_2 \,\text{erf}\,(\eta) + b^{(3)}_2$$
$$C^{(3)}_D = a^{(3)}_3 \,\text{erf}\,(\eta) + b^{(3)}_3$$

$\eta \ge \eta_3$

$$C^{(4)}_A - C^{(4)}_B = a^{(4)}_1 \,\text{erf}\,(\eta) + b^{(4)}_1$$
$$C^{(4)}_D = a^{(3)}_3 \,\text{erf}\,(\eta) + b^{(3)}_3$$

The problem is completely specified when the solid concentration is forced to vanish at the boundary upstream of a gap, i.e., by invoking a gradual precipitation front. The aqueous profiles are given in Table 8. The constants of integration for this problem, with the same initial and boundary conditions as Figure 2b are shown in Table 9, and the profiles are plotted in Figure 6b.

Discussion

General

All changes in aqueous concentration occur at small $\eta[= x/(2\sqrt{Dt})]$ because all aqueous profiles are functions only of erf (η), which is essentially constant for η greater than about 3.0. The transformation to η space maps all problem features for all time and space into a single diagram.

The velocity of a front, $v = (dx/dt)$, leads to an expression for the velocity of a moving boundary $v_{B_m} = \eta_m\sqrt{D/t}$. The larger the initial solid concentration, the smaller the value of η_m, and thus the slower the dissolution velocity. A problem with larger initial solid concentrations, all other things equal, will have slower front velocities and so the diffusion response will appear "compressed" into a smaller zone with steeper gradients.

Single-solid dissolution problems

For single-solid dissolution problems, the aqueous and solid profiles in the region containing the solid remain constant when, and only when, $C^I_A - C^I_B = C^J_A - C^J_B$, as plotted in Figure 7, as shown by Lichtner (1986a). We can show this mathematically by taking a linear combination of the concentration matching and Stefan conditions of Table 3, which gives $a_1 = 0$ for this case. The solid profile equation of Table 3 shows that the increase in solid concentration is proportional to $(a_1)^2$, and thus is constant. The initial condition for this trivial case appear on the $C^T_A = C^T_B$ line of Figure 3. Situations for which the above equality does not hold, as in Figure 2 and the diffusion part of Figure 4, exhibit nonconstant profiles with a peak in solid concentration at the dissolution front. Figure 2 also clearly shows the change in front position (i.e., dissolution velocity) as a func-

Table 9. Constants of Integration for the AB Dissolution Problem with a Gradual DB Precipitation Front

Initial Conditions

$$C_A^I = 2.0 \qquad C_B^I = 1.0 \qquad C_D^I = 0.4$$

Injected Conditions

$$C_A^J = 1.5 \qquad C_B^J = 0.3 \qquad C_D^J = 1.2$$

Solubility Product

$$K_{AB}^{sp} = 2.0 \qquad K_{DB}^{sp} = 0.5$$

For $S_{AB}^I = 0.05$

$$a_1^{(1)} = 0.5416 \qquad b_1^{(1)} = 1.5$$
$$a_2^{(1)} = 0.7176 \qquad b_2^{(1)} = 0.3$$
$$a_3^{(1)} = -0.8240 \qquad b_3^{(1)} = 1.2$$
$$a_2^{(2)} = -1.5416 \qquad b_2^{(2)} = 0.9$$
$$a_2^{(3)} = 0.8053 \qquad b_2^{(3)} = 0.2362$$
$$a_3^{(3)} = -0.7362 \qquad b_3^{(3)} = 1.1362$$
$$a_1^{(4)} = -0.2638 \qquad b_1^{(4)} = 1.2638$$

$$\eta_1 = 0.3094$$
$$\eta_2 = 0.6273$$
$$\eta_3 = 1.3410$$
$$S_{DB}^{(2)}|_{\eta_1} = 0.2422$$
$$S_{DB}^{(2)}|_{\eta_2} = 0.0$$
$$S_{AB}^{(4)}|_{\eta_3} = 0.05002$$

tion of the initial solid concentration. Numerical values for these front positions are in Table 4.

Dissolution problems with precipitation

Dissolution fronts are shocks but precipitation fronts need not be shocks. A shock precipitation front is always accompanied by a dissolution front. Gradual precipitation-only fronts occur and require an additional condition at moving boundaries, a new feature of this type of problem.

In problems with precipitation there are two different metasomatic structures. The initial solid concentration has a strong influence on the sequence (see Figures 6a and 6b). Figures 8–10 show the effect of the solubility product of the precipitating solid on the structure, showing a gradual precipitation front at high solubility and a shock precipitation/dissolution front at low solubility.

The velocity of dissolution fronts is directly affected by solid precipitation. The cases in Figures 2a and 6a have identical initial and injected conditions; the only difference is that species DB is allowed to precipitate in Figure 6a. The precipitation enhances dissolution of AB by providing a sink for B liberated by dissolution, and thus the front occurs at larger η (moves faster) than in the case with no DB precipitation. See Tables 4, 7 and 9 for numerical values of front positions.

Local maxima in aqueous profiles

Many of the aqueous profiles show marked peaks in concentration at a dissolution boundary (cf. the A^+ profile in Figures 2a, 6a, 8–10). Kopinsky et al. (1988) explain this phenomenon as an artifact of finite-rate kinetics, but our system is in local

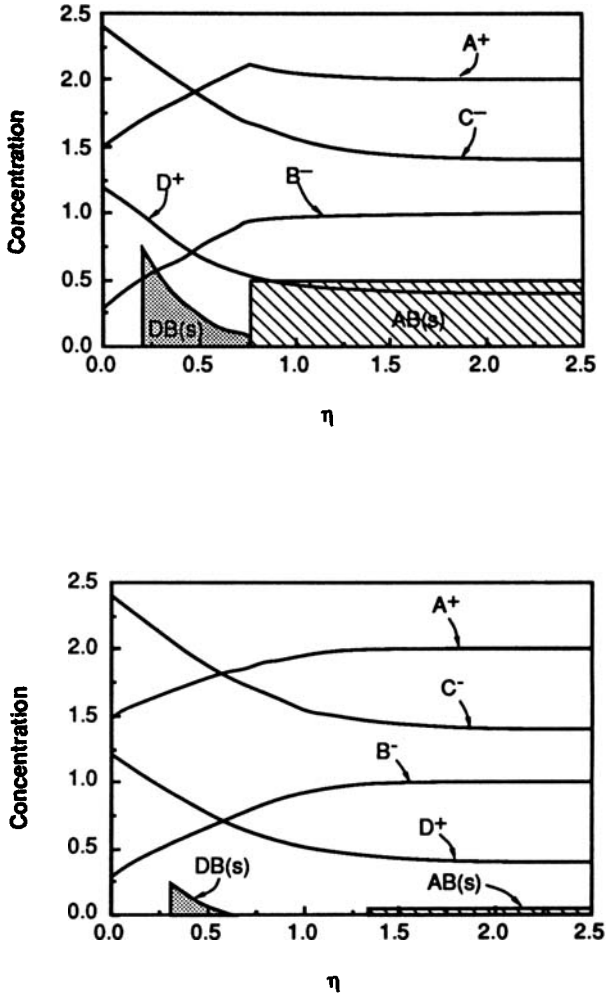

Figure 6. Solid and aqueous concentration profiles for the diffusion-dominated dissolution of solid AB with solid DB precipitation.

The two figures show the influence of initial solid concentration on the presence or absence of the intervening gap.

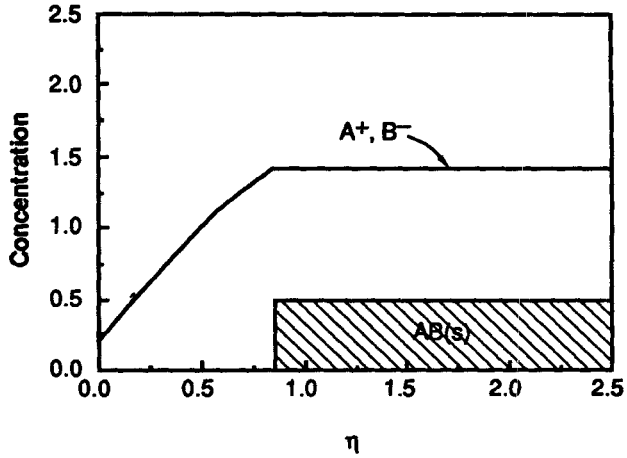

Figure 7. A trivial case where species A and B have the same initial and boundary concentrations, and thus follow the same diffusion path.

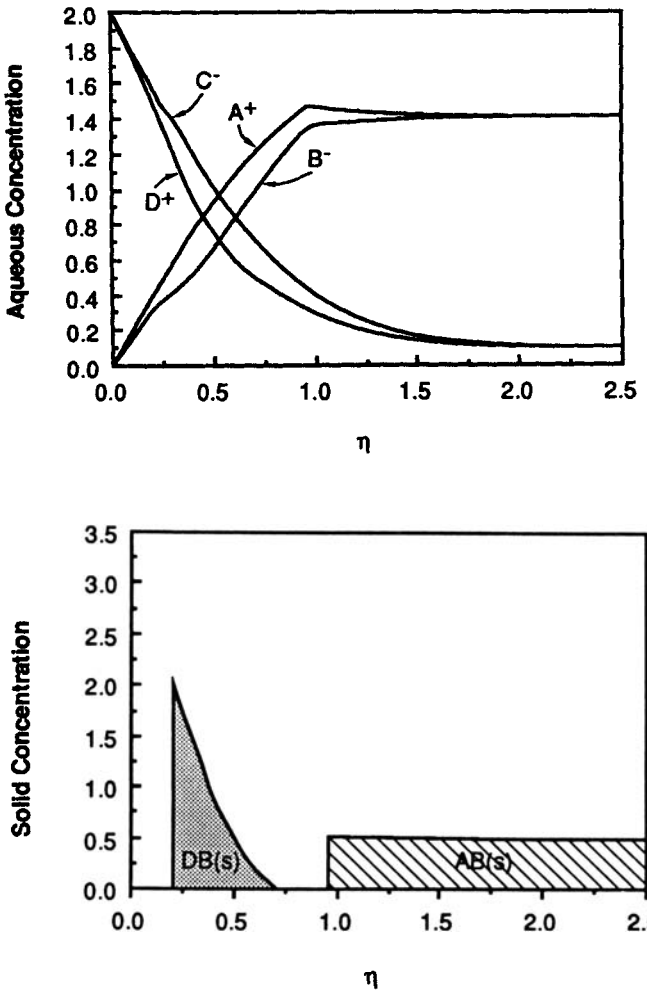

Figure 8. Solid and aqueous concentration profiles for $K_{DB}^{sp} = 0.5$, with initial conditions $C_A^I = C_B^I = 1.414$ and $C_C^I = C_D^I = 0.1$, and boundary conditions $C_A^J = C_B^J = 0.0$ and $C_C^J = C_D^J = 2.0$, with $K_{DB}^{sp} = 2.0$.

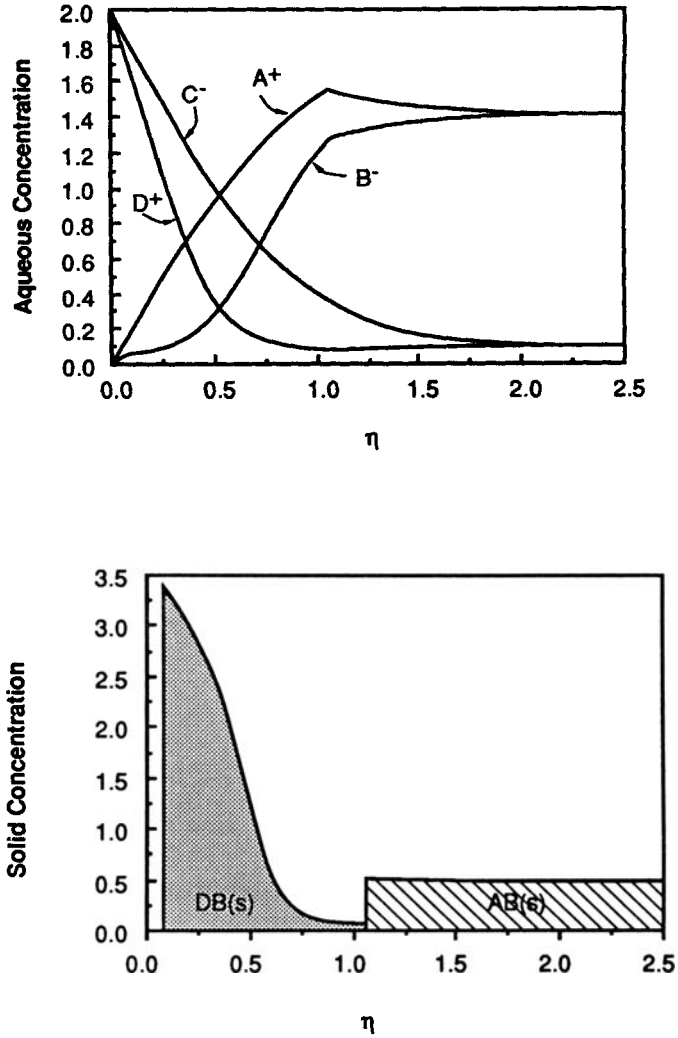

Figure 9. Solid and aqueous concentration profiles for $K_{DB}^{sp} = 0.1$, with all other conditions identical to Figure 8.

equilibrium so that argument is inapplicable here. Our interpretation, given primarily with reference to Figure 2a, is as follows. Species A^+ has a smaller overall driving force for diffusion, $C_A^I - C_A^J = 0.5$, than species B^-, $C_B^I - C_B^J = 0.7$. Thus, B^- will diffuse out of the medium more quickly than A^+. However, A^+ and B^- are added to the aqueous phase in a one-to-one ratio by solid dissolution. Since B^- diffuses out faster than A^+, there is a net accumulation of A^+ at the dissolution boundary. This accumulation is manifested in the peak in, for example, the aqueous A^+ concentration of Figure 2a, and also in the solid profile, which is not obvious on the scale of Figure 2a. (The integral describing the solid AB profile in Table 3 clearly shows AB increases as η approaches the dissolution boundary from the right.) Species A^+ is thus diffusing away from the dissolution boundary, both into as well as out of the permeable medium.

Comparison to convection-dominated problems

Throughout the text we have attempted to contrast convection-dominated and diffusion-dominated problems. Figures 3 and 4 do this for a specific AB dissolution problem, but we provide a more general comparison here.

Convection-dominated problems are less complicated than diffusion-dominated problems. The existence of coherence conditions (Riemann invariants) leads to the notion of composition path diagrams which can represent solutions for arbitrary initial and injected conditions. It is possible to compare specific convection- and diffusion-dominated problems, as does Figure 3, but the composition path diagram is not general for diffusion-dominated problems.

The nature of the transform variables for the two cases suggest that waves will migrate in proportion to time for convection-dominated cases. The same waves will travel in proportion to the square root of the product of the diffusion coefficient times time in diffusion-dominated cases.

All concentration changes are shocks in convection-dominated cases, and precipitation-only waves cannot occur (Novak et al., 1988).

Diffusion-dominated and convection-dominated problems can exhibit different mineral sequences. For diffusion-domi-

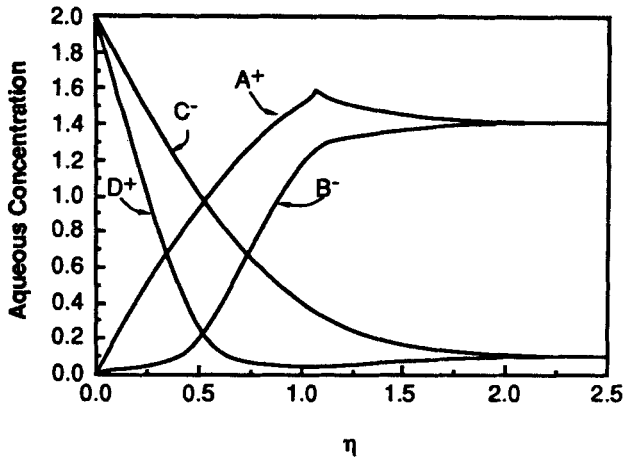

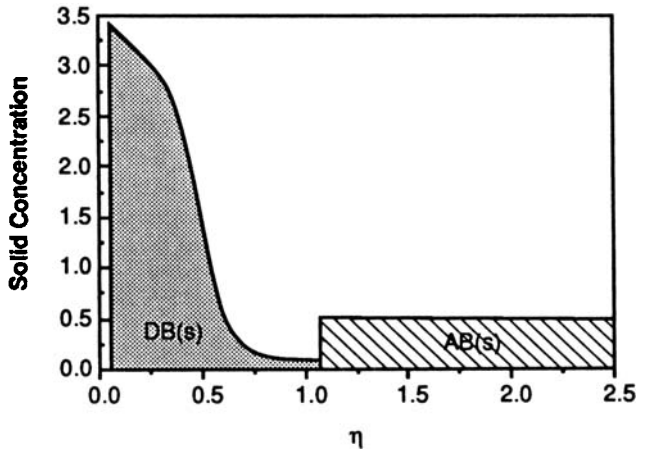

Figure 10. Solid and aqueous concentration profiles for $K^{sp}_{DB} = 0.05$, with all other conditions identical to Figures 8 and 9.

nated problems, it is possible for gaps to appear in the mineral sequence, where a region containing no solids is bounded in both directions by regions containing solids. Such gaps cannot occur in convection-dominated problems. Also, the mineral sequence in convection-dominated problems depends on the ratio of concentrations of initial solids and not the actual amount of the solids (Dria, 1988), whereas the mineral sequence in diffusion-dominated problems depends both upon the ratio of initial solid concentrations and the actual concentrations themselves.

Numerical Simulations for Dissolution of Hydroxyapatite

The numerical simulation scheme we used involved discretizing the material balance partial differential equation, Eq. 3, using forward-in-time, centered-in-space explicit finite differencing. This technique provides elemental totals at a series of node points in the medium, which are then flashed to determine aqueous and solid concentrations. The semi-infinite character of the system was achieved by choosing the number of node points

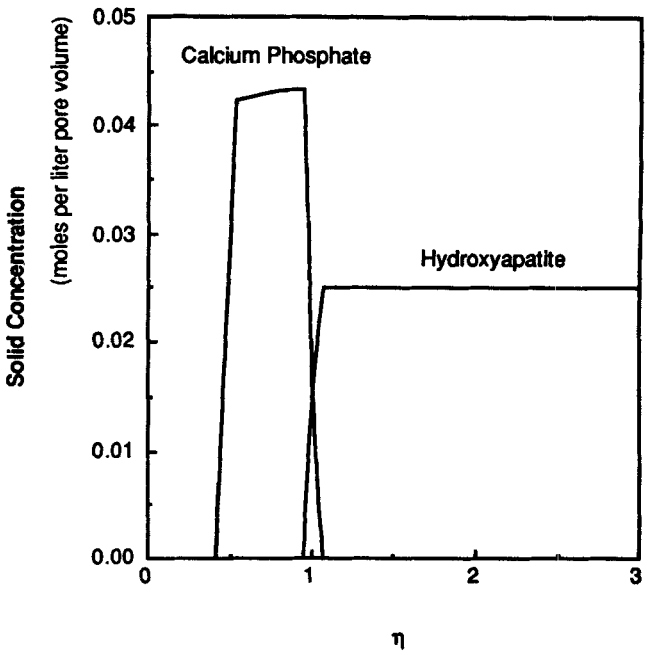

Figure 11. Solid concentration profiles from the numerical simulation of an experiment by Kim and Cussler (1987).

and the time step such that the initial condition always occurred at the right end of the medium (i.e., large η) and integrating until constant profiles in η-space were achieved (see Novak, 1989 for more details).

We have numerically simulated the physical system of hydroxyapatite, $Ca_5(PO_4)_3OH$, being dissolved by acid diffusion. The simulator, based on the algorithms used by Stohs (1986),

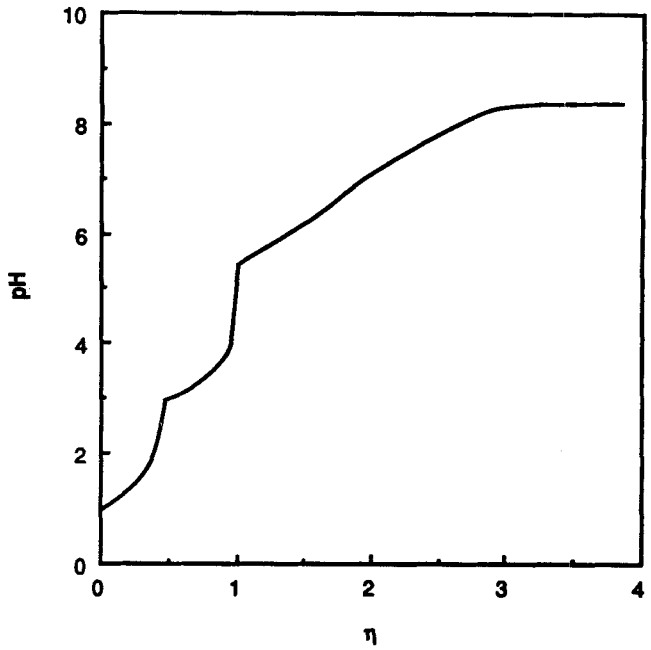

Figure 12. pH profiles from the numerical simulation of an experiment by Kim and Cussler (1987).

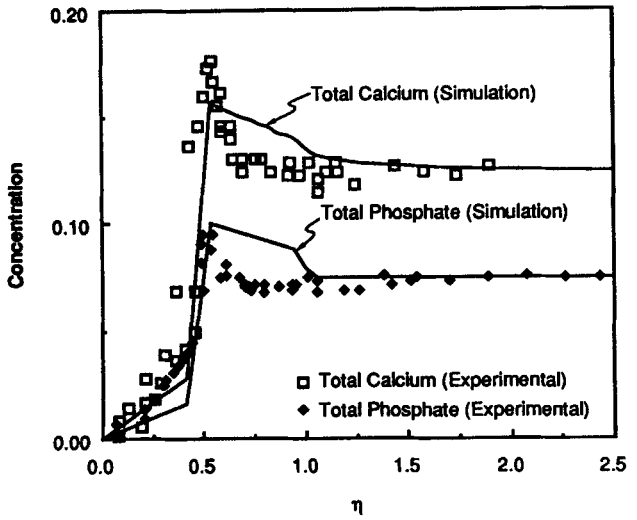

Figure 13. Total calcium and total phosphate concentrations (i.e., for both aqueous and solid phases) from the simulation of an experiment by Kim and Cussler (1987), whose data are superimposed.

accommodates intraaqueous reactions and multiple solids easily. For the simulation presented here we allowed the formation of the aqueous species H_2O, H^+, OH^-, Cl^-, HCl, H_3PO_4, $H2PO_4^-$, HPO_4^{2-}, PO_4^{3-}, Ca^{2+}, $CaOH^+$, $Ca(OH)_2$ and the minerals $Ca_5(PO_4)_3OH$(s) (hydroxyapatite), $Ca_3(PO_4)_2$(s) (calcium phosphate), $Ca(OH)_2$(s), $CaHPO_4$(s), $CaHPO_4 \cdot 2H_2O$(s), and $Ca(H_2PO_4)_2$(s).

The dissolution of hydroxyapatite suspended in aqueous gelatin was examined experimentally by Kim and Cussler (1987). We simulated Kim and Cussler's experimental conditions as closely as possible but encountered one significant difference. Using published thermodynamic data (Garrels and Christ, 1965; Stumm and Morgan, 1981) we were unable to make hydroxyapatite exist in pH = 4.5 solutions with an aqueous calcium to phosphate ratio of 5 to 3 as reported by Kim and Cussler. Therefore, we used an initial pH of 8.2. Perhaps the presence of the gelatin affected the pH profile; however, the calculated pH in the regions where dissolution and precipitation occurs is not too different from what is observed, so this discrepancy may not be very important. Figures 11 through 13 contain the results of our simulation.

As Figure 11 shows, calcium phosphate precipitates in a shock at the hydroxyapatite dissolution front at $\eta \approx 1.0$. The calcium phosphate then dissolves at $\eta \approx 0.5$. The pH profile in Figure 12 exhibits sharp changes at both of the (precipitation/)dissolution shocks and then gradually increases to the initial pH. Figure 13, showing elemental totals of calcium and phosphorus, is in good agreement with the total calcium and total phosphate figures of Kim and Cussler (1987), the data from which has been added to Figure 13. The solid profiles of Kim and Cussler were drawn from profiles of elemental totals at four time levels.

The gradual decrease in the concentration of calcium phosphate as the inlet is approached is a feature not indicated from the *ABCD* problem analysis and is probably caused by the more complicated equilibrium expressions and the intraaqueous reactions of the system. Still, similarities such as shock dissolution, dissolution/precipitation fronts, and constant profiles in η space are present in good agreement.

Conclusions

- The dissolution and precipitation of solids caused by diffusion into permeable media give rise to zones of minerals, separated by either abrupt or gradual changes in mineral concentration, which can be completely characterized by the sequence of solids.
- Problems with simple stoichiometry and negligible intraaqueous reaction can be solved analytically without assumptions.
- The analytical solution found here exhibits features (e.g., gradual precipitation-only fronts and mineral sequences which depend upon initial solid concentrations) not previously observed.
- Gaps between dissolution and precipitation-only fronts can occur.
- The velocity of a dissolution front is increased when its dissolution causes the precipitation of another solid.
- The analytical solution explains the appearance of shock dissolution and shock dissolution/precipitation fronts that appear in experimental results.
- Numerical simulation of a physical system closely mimics the experimental and analytical results.

Acknowledgment

This research was supported by the following sponsors: Elf Aquitaine, Norsk Hydro Research Centre, Imperial Chemical Industries, Texaco, Exxon Production Research Co., Sun Exploration and Production Co., Arco Oil and Gas Co., Shell Development Co., and the U.S. Dept. of Energy.

Dr. Schechter holds the Getty Oil Company Centennial Chair in Petroleum Engineering.

Dr. Lake holds the Shell Distinguished Chair and Halliburton Annual Professorship in Petroleum Engineering.

Notation

C, C_i = vector of length I of concentrations of the ith element in the aqueous phase
$\bar{C}, \bar{C}_i$ = vector of length I of concentrations of the ith element in the solid phase
D, d_{ij} = aqueous stoichiometric matrix, indicates the number of atoms of the ith element in the jth aqueous species
D_j = effective binary diffusion coefficient for the jth aqueous species
D_o = average effective binary diffusion coefficient
F, f_{ik} = I-by-K solid stoichiometric matrix, indicates the number of atoms of the ith element in the kth solid species
H = linear differential operator
I = total number of chemical elements
J = total number of aqueous species
K = total number of minerals
K_r = number of solids in the rth region
M = number of dissolution, precipitation, and dissolution/precipitation boundaries
P, p_{ij} = I-by-I elementary matrix, Eqs. 11 to 13
Q = ρ_r-by-K submatrix of real constants
R_r = the rth region
S, S_k = vector of length K of concentration of the kth mineral

Greek letters

Δ^r = K-by-K diagonal matrix indicating the presence or absence of solids in the rth region, Eq. 9
η = dimensionless Boltzmann transform variable

η_m = position of the mth dissolution, precipitation, or dissolution/precipitation boundary
ρ_r = rank $(F\Delta')$
σ_j = concentration of the jth aqueous species

Superscript

r = indicates a quantity in the rth region

Literature Cited

Bird, R. B., W. E. Stewart, and E. N. Lightfoot, *Transport Phenomena*, Wiley, New York (1960).

Bryant, S. L., "Wave Behavior in Reactive Flow through Permeable Media," PhD Diss., Univ. of Texas, Austin (1986).

Bryant, S. L., R. S. Schechter, and L. W. Lake, "Interactions of Precipitation/Dissolution Waves and Ion Exchange in Flow through Permeable Media," *AIChE J.*, **32**, 751 (May, 1986).

———, "Mineral Sequences in Precipitation/Dissolution Waves," *AIChE J.*, **33**, 1271 (Aug., 1987).

Crank, J., *Free and Moving Boundary Problems*, Clarendon Press, Oxford (1984).

Cussler, E. L., "Dissolution and Reprecipitation in Porous Solids," *AIChE J.*, **28**, 500 (May, 1982).

Cussler, E. L., J. Kopinsky, and J. A. Weimer, "The Effect of Pore Diffusion on the Dissolution of Porous Mixtures," *Chem. Eng. Sci.*, **38**, 2027 (1983).

Dria, M. A., "Chemical and Thermochemical Wave Behavior in Multiphase Fluid Flow Through Permeable Media: Wave-Wave Interactions," PhD Diss., Univ. of Texas, Austin (1988).

Garrels, R. M., and C. L. Christ, *Solutions, Minerals, and Equilibria*, Harper and Row, New York (1965).

Helfferich, F., "The Theory of Precipitation/Dissolution Waves," *AIChE J.*, **35**, 75 (Jan., 1989).

Helfferich, F., and A. Katchalsky, "A Simple Model of Interdiffusion with Precipitation," *J. Phys. Chem.*, **74**, 308 (Jan., 1970).

Helfferich, F., and G. Klein, *Multicomponent Chromatography*, Marcel Dekker, New York (1970).

Kim, J. L., and E. L. Cussler, "Dissolution and Reprecipitation in Model Systems of Porous Hydroxyapatite," *AIChE J.*, **33**, 705 (May, 1987).

Kopinsky, J., R. Aris, and E. L. Cussler, "Theories of Precipitation Induced by Dissolution," *AIChE J.*, **34**, 2005 (Dec., 1988).

Lake, L. W., *Enhanced Oil Recovery*, Prentice-Hall, Englewood Cliffs, NJ (1989).

Lichtner, P. C., "Continuum Model for Simultaneous Chemical Reactions and Mass Transport in Hydrothermal Systems," *Geochim. et Cosmochim. Acta*, **49**, 779 (1985).

Lichtner, P. C., E. H. Oelkers, and H. C. Helgeson, "Exact and Numerical Solutions to the Moving Boundary Problem Resulting from Reversible Heterogeneous Reactions and Aqueous Diffusion in a Porous Medium," *J. Geophys. Res.*, **B 91:7**, 7531 (1986a).

———, "Interdiffusion with Multiple Precipitation/Dissolution Reactions: Transient Model and the Steady-state Limit," *Geochim. et Cosmochim. Acta*, **50**, 1951 (1986b).

Novak, C. F., "Metosomatic Patterns Produced by Infiltration or Diffusion in Permeable Media," PhD Diss., University of Texas, Austin (1989).

Novak, C. F., R. S. Schechter, and L. W. Lake, "Rule-based Mineral Sequences in Geochemical Flow Processes," *AIChE J.*, **34**, 1607 (Oct., 1988).

Perkins, T. K., and O. C. Johnston, "A Review of Diffusion and Dispersion in Porous Media," *SPE J.*, 70 (Mar., 1963).

Rhee, H. K., R. Aris, and N. R. Amundson, "On the Theory of Multicomponent Chromatography," *Phil. Trans. Roy. Soc. Lond.*, **A267**, 419 (1970).

Schechter, R. S., S. L. Bryant, and L. W. Lake, "Isotherm-free Chromatography: Propagation of Precipitation/Dissolution Waves," *Chem. Eng. Comm.*, **58**, 353 (1987).

Smith, W. R., and R. W. Missen, *Chemical Reaction Equilibrium Analysis: Theory and Algorithms*, Wiley, New York (1982).

Stohs, M., "A Study of Metal Ion Migration in Soils from Drilling Mud Pit Discharges," MS Thesis, Univ. of Texas, Austin (1986).

Strang, G., *Linear Algebra and Its Applications*, 2nd ed., Academic Press, New York (1980).

Stumm, W., and J. J. Morgan, *Aquatic Chemistry*, 2nd ed., Wiley, New York (1981).

Walsh, M. P., "Geochemical Flow Modelling," PhD Diss., Univ. of Texas, Austin (1983).

Walsh, M. P., S. L. Bryant, R. S. Schechter, and L. W. Lake, "Precipitation and Dissolution of Solids Attending Flow through Porous Media," *AIChE J.*, **30**, 317 (Mar., 1984).

Walsh, M. P., L. W. Lake, and R. S. Schechter, "A Description of Chemical Precipitation Mechanisms and Their Role in Formation Damage During Stimulation By Hydrofluoric Acid," *J. Pet. Tech.*, 2097 (Sept., 1982).

Appendix: Proof of Gradual (Nonshock) Precipitation Front Solution

The following analysis demonstrates that a shock precipitation-only front cannot occur by showing that the solid concentration at the leading edge of the precipitation front must be zero. Since solid DB is not present in region R_3 (see Figure 5b),

$$C_D^{(3)}\, C_B^{(3)} \le K_{DB}^{sp}$$

Expanding C_D and C_D in a Taylor series about η_2 truncated to first-order terms and dropping the region superscript gives

$$\{C_D|_{\eta_2^+} + C'_D|_{\eta_2^+}(\eta - \eta_2)\}\{C_B|_{\eta_2^+} + C'_B|_{\eta_2^+}(\eta - \eta_2)\} \le K_{DB}^{sp}$$

Multiplying and dropping second-order terms in $(\eta - \eta_2)$ yields

$$\{C_D|_{\eta_2^+}\}\{C_B|_{\eta_2^+}\} + \{C'_D C_B + C'_B C_D\}|_{\eta_2^+}(\eta - \eta_2) \le K_{DB}^{sp}$$

since

$$\{C_D|_{\eta_2^+}\}\{C_B|_{\eta_2^+}\} = K_{DB}^{sp}$$

we have

$$\{C'_D C_B + C'_B C_D\}|_{\eta_2^+}(\eta - \eta_2) \le 0$$

and since $\eta - \eta_2$ is always positive

$$\{C'_D C_B + C'_B C_D\}|_{\eta_2^+} \le 0$$

Defining the variables

$$LC \equiv [a_4 \operatorname{erf}(\eta_2) + b_4]$$
$$SQ \equiv \sqrt{[a_4 \operatorname{erf}(\eta_2) + b_4]^2 + 4K_{DB}^{sp}}$$

the Stefan conditions on D and B at η_2 are

$$C'_D|_{\eta_2^+} = 2\eta_2 \bar{C}_{DB}|_{\eta_2^-} + \frac{a_4}{2}\frac{LC + SQ}{SQ}\frac{d[\operatorname{erf}(\eta)]}{d\eta}\bigg|_{\eta_2^+}$$

$$C'_B|_{\eta_2^+} = 2\eta_2 \bar{C}_{DB}|_{\eta_2^-} + \frac{a_4}{2}\frac{LC - SQ}{SQ}\frac{d[\operatorname{erf}(\eta)]}{d\eta}\bigg|_{\eta_2^+}$$

with the concentration matching conditions

$$C_D|_{\eta_2^+} = \frac{LC + SQ}{2} = C_D|_{\eta_2^-}$$

$$C_B|_{\eta_2^+} = \frac{-LC + SQ}{2} = C_B|_{\eta_2^-}$$

With substitution and simplification the inequality becomes

$$2\eta_2 \bar{C}_{DB}|_{\eta_2^-} \sqrt{[a_4 \text{ erf}(\eta_2) + b_4]^2 + 4K_{DB}^{sp}} \leq 0$$

which can only be satisfied for

$$\bar{C}_{DB}|_{\eta_2^-} = 0$$

since the positive square root must be taken to ensure nonnegative aqueous concentrations. Since the solid concentration is zero at the boundary as approached from both sides, the right-hand-side of the Stefan condition, Eq. 6, is zero and thus the first derivatives of the aqueous concentrations of species comprising the precipitating solid are continuous.

Manuscript received Sept. 16, 1988, and revision received Mar. 28, 1989.